Supplementary Information

for

Enhanced relaxivity of Gd^{III}-complexes with HP-DO3A-like ligands upon the activation of the intramolecular catalysis of the prototropic exchange

Luciano Lattuada,[a,*] Dávid Horváth,[b] Sonia Colombo Serra,[c] Alberto Fringuello Mingo,[c] Paolo Minazzi,[d] Attila Bényei,[b] Attila Forgács,[e] Franco Fedeli,[d] Eliana Gianolio,[f] Silvio Aime,[f] Giovanni B. Giovenzana,[d,g] Zsolt Baranyai[c,*]

[a] Innovation Hub, Bracco SpA, Via Caduti di Marcinelle 13, 20134 Milano, Italy

[b] Department of Physical Chemistry, University of Debrecen, H-4010, Debrecen, Egyetem tér 1., Hungary

[c] Bracco Research Center, Bracco Imaging SpA, Via Ribes 5, 10010 Colleretto Giacosa (TO), Italy

[d] CAGE Chemicals, Via Bovio 6, 28100 Novara, Italy

[e] MTA-DE Redox and Homogeneous Catalytic Reaction Mechanisms Research Group, Egyetem tér 1, Debrecen, H-4032 Hungary

[f] Department of Molecular Biotechnologies and Health Science, University of Turin, Via Nizza 52, 10125, Turin, Italy

[g] Dipartimento di Scienze del Farmaco, Università del Piemonte Orientale "A. Avogadro", Largo Donegani 2/3, Novara, Italy

Content:

I. Synthesis of L_1 and L_2

Chemicals and solvents were obtained from commercial sources and were used without further purification. Compounds **1**[S1] and tri-*t*-butyl phosphite[S2] were synthesized as reported in literature procedures. TLC was performed with Merck silica gel 60 TLC plates F254 and visualized by UV light, 1% $KMnO_4$ in 1M NaOH or ceric ammonium molybdate. Flash chromatography was carried out on silica gel 60 (230–400 mesh). Melting points were determined on a Buchi 540 apparatus and are uncorrected. ^1H and ^{13}C-NMR spectra were recorded on a Jeol Eclipse ECP300 instrument operating at 7.05 T. Mass spectra were recorded with a ThermoFinnigan TSQ700 triple-quadrupole instrument equipped with an electrospray ionization source. Elemental analyses were performed by Redox laboratories, Monza, Italy.

10-[2-Hydroxy-3-[(phenylmethyl)amino]propyl]-1,4,7,10-tetraazacyclododecane-1,4,7-triacetic acid tris(1,1-dimethylethyl) ester (2)

Benzaldehyde (3.18 g; 30 mmol) and acetic acid (9 mL) were added to a solution of compound **1** (19.4 g; 30 mmol) in EtOH (100 mL) and the reaction mixture was stirred for 16 h. The solution was then cooled to 0-5°C and sodium borohydride (7.5 g; 210 mmol) was added in small portions. The reaction was maintained at room temperature for 2 h then cooled and diluted with water (200 mL). The organic solvent was evaporated, and the pH of the remaining aqueous solution was increased to pH 11 with 2N NaOH (30 mL), then extracted with dichloromethane. After evaporation of the organic solvent the monoalkylated intermediate **2** was obtained as an oil (17.0 g, 25 mmol, 83%). ^1H NMR (300 MHz, $CDCl_3$) δ (ppm): 1.37 (s, 9H), 1.38 (s, 18H), 1.97-3.31 (m, 28H), 3.78 (d, 1H, J = 13.5Hz), 3.83 (d, 1H, J = 13.5Hz), 3,93 (bt, 1H), 7.17 (bt, 1H), 7.23 bt, 2H), 7.32 (bd, 2H). ^{13}C NMR (75 MHz, $CDCl_3$) δ (ppm): 28.0 ($2CH_3$), 28.2 (CH_3), 48.5 (b, $2CH_2$), 52.0 (CH_2), 52.2 (CH_2), 53.2 (CH_2), 55.7 (CH_2), 55.9 (CH_2), 56.1 (CH_2), 64.5, 65.4 (CH,CH_2), 81.8 (2C), 82.1 (C); 127.2 (CH), 128.4 (CH), 128.5 (CH), 138.2 (C), 172.3 (C), 172.7 (2C). MS(ESI^+) calculated for: $C_{36}H_{63}N_5O_7$ 677.47, found 678.54 (MH^+), 700.45 (MNa^+), 622.37 (MH^+-*t*Bu), 566.34 (MH^+- 2 *t*Bu), 510.30 (MH^+- 3 *t*Bu), 255.69 ($M+2H^+$- 3 *t*Bu).

10-[3-[[[Bis(1,1-dimethylethoxy)phosphinyl]methyl](phenylmethyl) amino]-2-hydroxypropyl]-1,4,7,10-tetraazacyclododecane-1,4,7-triacetic acid tris(1,1-dimethylethyl) ester (3)

Paraformaldehyde (1.17 g; 39 mmol) and tri-*t*-butyl phosphite (10.3 g; 34 mmol) were added to compound **2** (23.4 g; 34 mmol) and the obtained mixture was heated at 70 °C for 3 h. During this time additional tri-*t*-butyl phosphite was added after 1 h (3 g) and 2 h (1.5 g), respectively. The mixture was evaporated under vacuum to get a residue that was dissolved in dichloromethane and purified by flash-chromatography (eluent: dichloromethane/MeOH = 4:1) to obtain intermediate **3** (23.9 g, 27 mmol, 79%). ^{1}H NMR (300 MHz, $CDCl_3$) δ (ppm) 1.34-1.43 (m, 45H), 1.90-3.40 (m, 22H), 3.63 (m, 1H), 3.67 (s, 2H), 3.70-3.77 (m, 5H), 3.84 (d, 1H, J = 13.3 Hz), 4.25 (bs, 1H), 7.13-7.26 (m, 5H); ^{13}C NMR (75 MHz, $CDCl_3$) δ (ppm): 172.8 (C), 172.5 (C), 171.8 (C), 138.3 (C), 128.7 (CH), 128.3 (CH), 127.2 (CH), 82.6 (C), 82.0 (C), 81.8 (C), 81.5 (C), 65.2 (CH_2), 61.7 (CH_2), 61.6 (CH_2), 61.5 (CH_2), 56.0 ($2CH_2$), 55.5 (CH_2), 52.1 (CH_2), 51.3 (dCH_2, J = 168 Hz), 49.6 ($3CH_2$), 30.3 (bCH_3), 28.9 (CH_3), 28.8 ($2CH_3$). MS(ESI+) calculated for $C_{45}H_{82}N_5O_{10}P$: 883.58, found: 884.59 (MH^+), 906.61 (MNa^+), 828.58 (MH^+-*t*Bu).

10-[2-Hydroxy-3-[(phenylmethyl)(phosphonomethyl)amino]propyl]-1,4,7,10-tetraazacyclododecane-1,4,7-triacetic acid (L_1)

Trifluoroacetic acid (30 mL) was added to a solution of intermediate **3** (16.3 g; 18 mmol) in dichloromethane (150 mL). The mixture was evaporated, the residue was solubilized in neat TFA (60 mL), and triisopropylsilane (0.1 mL) was added. The obtained mixture was maintained under stirring for 72 h, then diluted with ethyl ether (450 mL) obtaining the precipitation of a solid that was filtered and purified by chromatography on Amberchrome CG161M column (eluent: gradient of water/MeCN) obtaining the desired ligand **L_1** (5.3 g, 8.8 mmol 49%). ^{1}H NMR (300 MHz, $CDCl_3$) δ (ppm): 7.48 (m, 2H), 7.42 (m, 3H), 4.12 (m, 1H), 3.84 (bt, 2H), 3.69 (bt, 2H), 3.57-2.43 (m, 26H); ^{13}C NMR (75 MHz, $CDCl_3$) δ (ppm): 174.8 (C), 170.5 (2C), 131.7 (C), 130.3 (CH), 129.4 (CH), 67.0 (CH), 59.6 (CH_2), 57.6 (CH_2), 56.7 (CH_2), 56.2 (CH_2), 52.3 (dCH_2, J = 150 Hz), 51.2 (CH_2), 51.1 (CH_2), 49.3 (CH_2), 48.6 (CH_2); MS(ESI+) calculated for $C_{25}H_{42}N_5O_{10}P$: 603.27; found 604.17 (MH^+), 560.17 (MH^+-CO_2).

Gadolinium complex of L_1 (GdL_1)

Gadolinium chloride hexahydrate (0.93 g, 2.5 mmol) was added to a solution of ligand **L_1** (1.6 g; 2.54 mmol) in water (20 mL) and the pH of the obtained solution was slowly increased to pH 6.5-7 with 2 N NaOH. The obtained solution was stirred at room

temperature for 4 h then filtered on a Millipore HA 0.45 μm filter, concentrated and purified by chromatography on Amberchrome CG161M column (eluent: water/MeCN gradient) obtaining of the gadolinium complex **GdL_1** (1.56 g, 2 mmol, 79%). Anal. Calcd for $C_{25}H_{38}GdN_5NaO_{10}P$: C, 38.51; H, 4.91; N, 8.98; Gd, 20.16; Na, 2.95; P, 3.97. Found: C, 38.69; H, 4.84; N, 8.89; Gd, 20.62, Na, 2.83; P, 3.90.

10-[3-[[1-(Diethoxyphosphinyl)-3-phenylpropyl]amino]-2-hydroxypropyl]-1,4,7,10-tetraazacyclododecane-1,4,7-triacetic acid tris(1,1-dimethylethyl) ester (4)

Compound **1** (14.9 g, 25 mmol), 3-phenylpropionaldeyde (3.30 mL, 26 mmol) and diethylphosphite (3.90 mL, 30 mmol) were mixed and heated at 80 °C for 8h. The crude reaction mixture was purified by silica gel column chromatography (dichloromethane/2-propanol: 95/5). The fractions containing the pure product were collected and evaporated to give the product **4** as a colourless oil. (16.8 g, 20 mmol, 80%). ^{1}H NMR (300 MHz, $CDCl_3$) δ (ppm): 1.09-1.23 (m, 6H, CH_3), 1.32-1.33 (2s, 27H, CH_3), 1.73-3.30 (m, 31H, CH_2 -CH), 3.46 (bs, 1H, CH), 3.65-4.11 (m, 4H, CH_2), 6.92-7.22 (m, 5H, CH_2). ^{13}C NMR (75 MHz, $CDCl_3$) δ (ppm): 16.5, 16.6, 16.8', 16.9' (CH_3), 27.8, 27.9', 28.1, 28.2' (CH_3), 31.4, 31.9', 32.1', 32.3 (CH_2), 48.4, 48.7, 48.8, 48.9, 50.7, 51.2, 52.0, 52.4, 52.6, 53.2, 53.5, 53.6 (CH_2), 53.6, 53.7' (CH), 55.5, 55.9, 56.3, 58.7, 58.8, 61.9, 62.0, 62.1 (CH_3), 66.3 (CH), 81.0', 81.7, 81.9, 82.0' (C), 125.8, 125.9, 128.4, 128.5 (CH), 141.3, 170.9', 171.9, 172.3, 172.8' (C). MS(ESI$^+$) calculated for: $[C_{42}H_{76}N_5O_{10}P]^+$ 841.53, found 842.2.

(') Diastereomeric mixture.

10-[2-Hydroxy-3-[(3-phenyl-1-phosphonopropyl)amino]propyl]-1,4,7,10-tetraazacyclododecane-1,4,7-triacetic acid (L_2)

A solution of bromotrimethylsilane (25.90 mL, 196 mmol) in dichloromethane (50 mL) was added dropwise to product **4** (16.5 g, 19.6 mmol) dissolved in dichloromethane (100 mL). The reaction was stirred overnight at room temperature. The solvent was evaporated and trifluoroacetic acid (50 mL) was added dropwise keeping the reaction in an ice bath. The reaction was then stirred at room temperature for 12 h. The solvent was evaporated, and the crude product was purified by elution on XAD 1600 resin. The product was charged on resin at acid pH and the salts and impurities were washed out with deionized water. The product was eluted with a water/MeOH gradient starting from 99-1 (v/v). The fractions containing the product

were collected to obtain the ligand **L_2** as a white solid (5.5 g, 8.9 mmol, 45%). ^{1}H NMR (300 MHz, D_2O) δ (ppm): 1.85-2.38 (m, 2H, CH_2), 2.45-4.12 (m, 30 H, CH_2-CH), 7.27-7.34 (m, 5 H, CH). ^{13}C NMR (75 MHz, D_2O) ä (ppm): 29.1-29.4-31.9-32.0-32.1-48.8-49.6-49.8-50.5-51.2-53.6 (CH_2), 54.4-54.6 (CH), 55.2-56.3-56.5-56.6 (CH_2), 126.7-128.8-129.0 (CH), 141.1-170.7-171.0-174.6 (C). ^{31}P NMR (75 MHz, D_2O) δ (ppm): 11.8. MS(ESI+) calculated for: $[C_{26}H_{44}N_5O_{10}P]^+$ 617.28, found 618.80. HPLC R_t= 6.31-6.87 min., diastereomeric mixture, purity 98.9% (combined assay).

Gadolinium complex of L_2 (GdL_2)

Ligand **L_2** **(**3.20 g, 5.2 mmol) was suspended in deionized water (40 mL) and NaOH (0.42 g, 10.4 mmol) was added. Freshly prepared $Gd(OH)_3$ (starting from 1.93 g, of $GdCl_3 \cdot 6H_2O$, 5.2 mmol) was added. The opalescent suspension was stirred at 80°C until complete solution was obtained (about 24h). The solution was then filtered on 0.25 μm Millipore filters and evaporated under reduced pressure. The crude product was purified by elution on XAD 1600 resin. The product was charged on resin at pH=7 and the salts and impurities were washed out with deionized water. The product was eluted with a water/MeOH gradient starting from 98-2 (v/v). The fractions containing the product were collected, redissolved in deionized water (5mL) and precipitated with acetone (50 mL) for 3 times, then the solid was dried under vacuum to obtain **GdL_2** as a white powder (2.3 g, 3.5 mmol, 67%). Anal. Calcd for $C_{26}H_{39.5}GdN_5Na_{1.5}O_{10}P$: C, 38.79; H, 4.96; N, 8.70; Gd, 19.54; Na, 4.28; P, 3.85. Found: C, 38.94; H, 4.76; N, 8.70; Gd, 19.50, Na, 3.79; P, 4.00. MS(ESI-) calculated for: $[C_{26}H_{40}GdN_5O_{10}P]^-$ 771.17, found 771.34.

II. Protonation and complexation equilibria of L_1 and L_2 ligands

II.1. Acid-base properties of L_1 and L_2 ligands.

The protonation constants, defined by Equation (S1), have been determined by pH-potentiometry and ^{1}H-NMR spectroscopy.

$$K_i^H = \frac{[H_iL]}{[H_{i-1}L][H^+]} \qquad (S1)$$

where i=1, 2…6. The protonation sequence of **L_1** and **L_2** has been determined by ^{1}H-NMR spectroscopy, recording the chemical shift variations of the non-labile protons as a function of pH. The ^{1}H-NMR titration curves (Figures S1 and S2) display sharp changes at certain pH values, which are related to the protonation/deprotonation of the ligand. Since the protonation/deprotonation is fast on the NMR time scale, the chemical shifts of the observed signals represent a weighted average of the shifts of the different species involved in a specific protonation step (Eq. (S2)):[S3]

$$\delta_{obs} = \sum x_i \delta^{H_iL} \qquad (S2)$$

where, δ_{obs} is the observed chemical shift of a given signal (^{1}H and ^{31}P), x_i and δ^{H_iL} are the molar fraction and the chemical shift of the involved species, respectively. The observed chemical shifts (δ_{obs}) have been fitted to the Eq. (S2), respectively (the molar fractions x_i and the concentration of the different protonated species have been expressed by the protonation constants K_i^H, Eq. (S1)). The fittings of the experimental data points are shown in Figures S1 and S2. The obtained logK_i^H values are listed in Table S1.

Table S1. Protonation constants of **L_1**, **L_2**, **HP-DO3A** and **HPA-DO3A** at 25°C

	L_1		**L_2**		**HP-DO3A**[a]	**HPA-DO3A**[b]
I	0.15 M NaCl				0.1 M Me_4NCl	0.15 M NaCl
Method	pH-pot	^{1}H/ ^{31}P	pH-pot	^{1}H/ ^{31}P	pH-pot	pH-pot
logK_1^H	**9.50 (3)**	**9.58 (5)**	**9.93 (1)**	**10.10 (4)**	11.96	8.96
logK_2^H	9.30 (2)	9.11 (5)	9.10 (1)	9.24 (3)	9.43	9.07
logK_3^H	8.51 (2)	8.67 (2)	8.82 (1)	9.00 (5)	4.30	4.22
logK_4^H	**5.50 (3)**	**5.51 (3)**	**5.79 (2)**	**5.72 (4)**	3.26	2.64
logK_5^H	4.29 (4)	4.40 (8)	4.16 (2)	–	–	1.25
logK_6^H	2.49 (3)	2.18 (6)	2.34 (2)	–	–	–
logK_7^H	1.50 (4)	–	1.04 (4)	–	–	–

[a] Ref. [S4], [b] Ref. [S5]

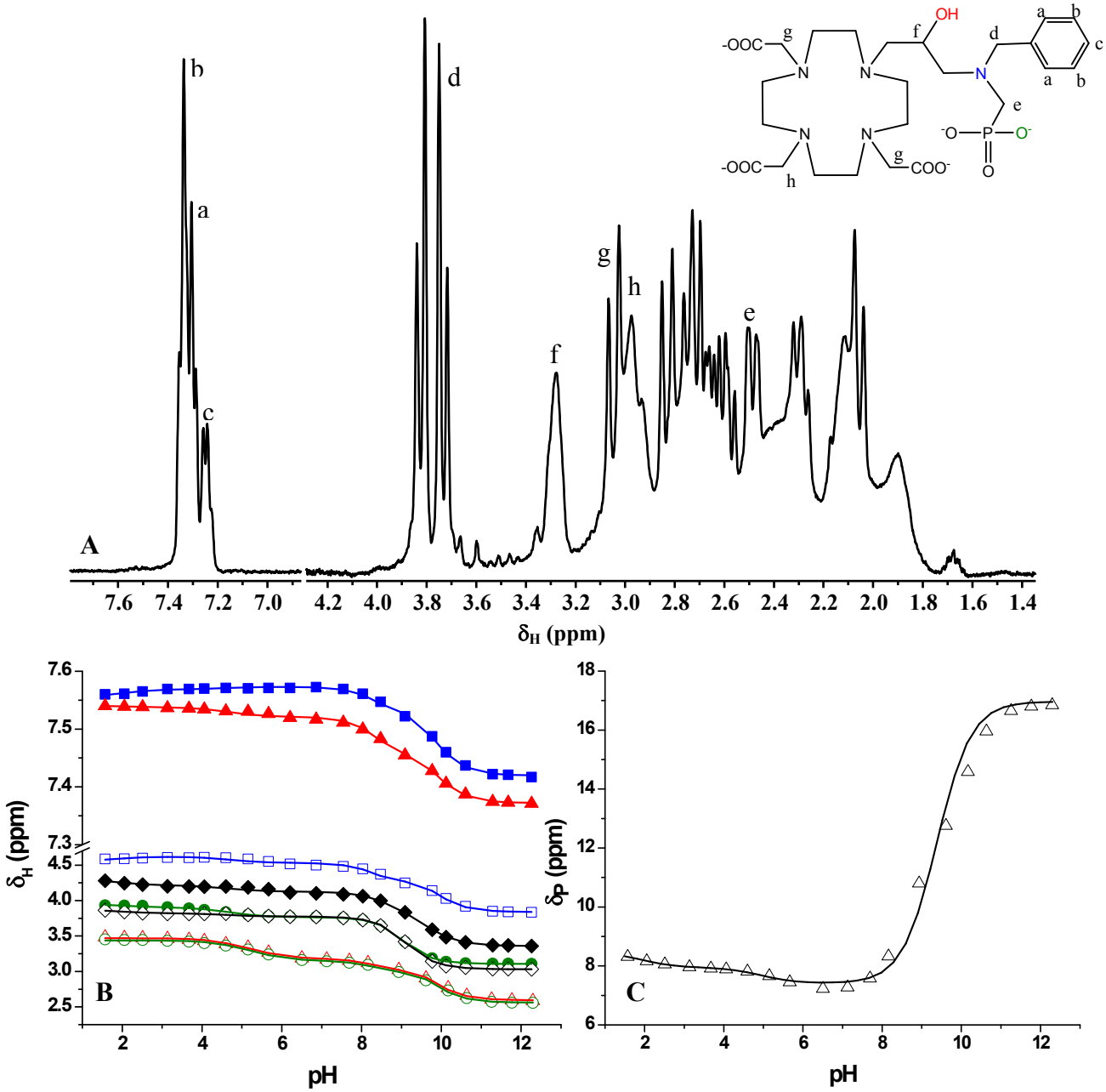

Figure S1. ^{1}H-NMR spectra of $\mathbf{L_1}$ (**A**) and the chemical shifts of the different protons (**B**) and phosphorous atom (**C**) as a function of pH. The solid lines and the symbols represent the the calculated and the experimental chemical shift values, respectively. (A: pH=12.29; B: a (▲), b (■), d (□), e (○, ❒), f (♦), g (●) and h (❋), [$\mathbf{L_1}$]=0.02 M, 0.15 M NaCl, 25°C)

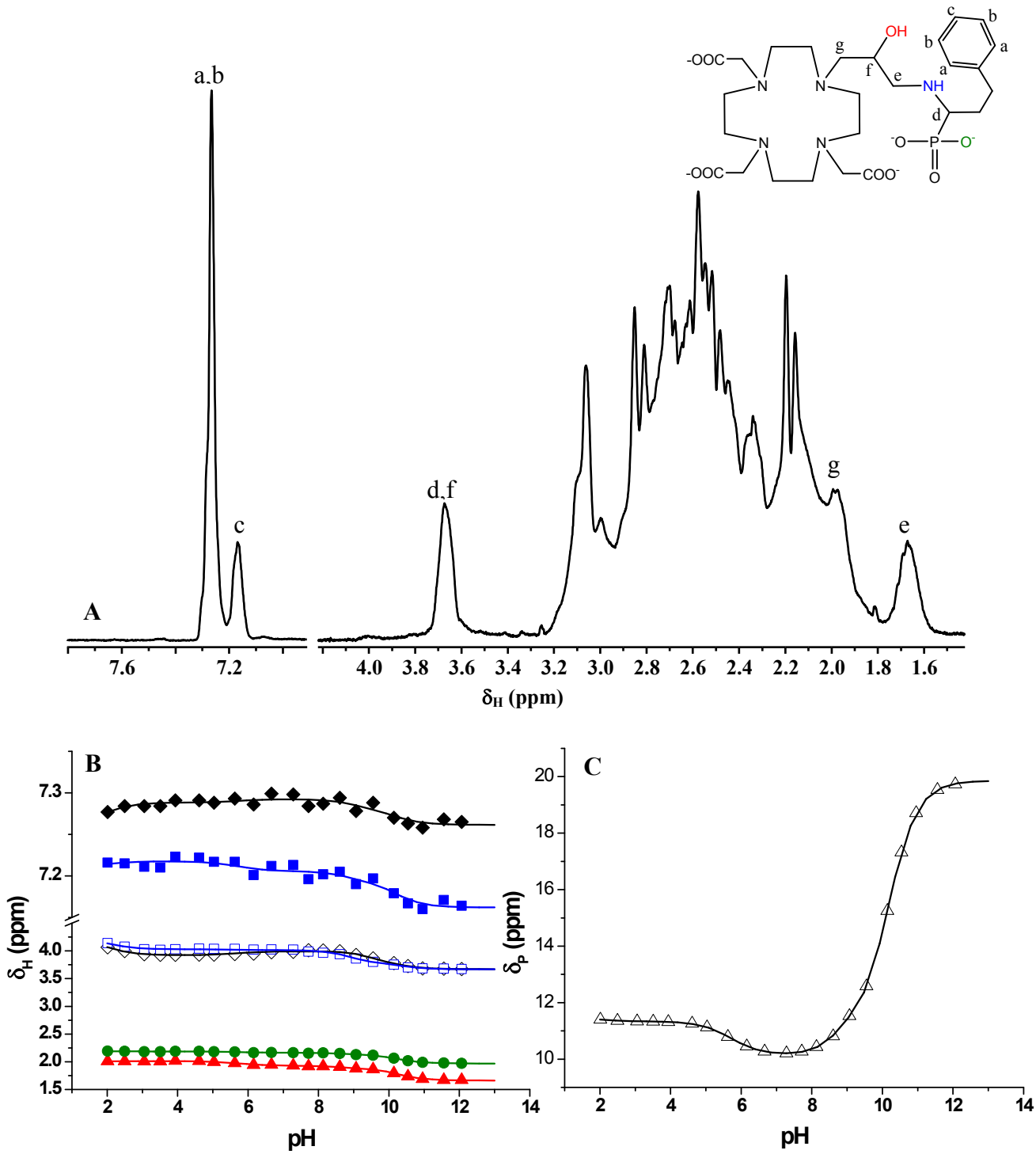

Figure S2. ^{1}H-NMR spectra of $\mathbf{L_2}$ (**A**) and the chemical shifts of the different protons (**B**) and phosphorous atom (**C**) as a functi on of pH. The solid lines and the symbols represent the the calculated and the experimental chemical shift values, respectively. (A: pH=12.06; B: a,b (♦), c (■), d (❋), e (▲), f (□) and g (●), [$\mathbf{L_2}$]=0.02 M, 0.15 M NaCl, 25°C)

The ^{1}H-NMR spectra of $\mathbf{L_1}$ and $\mathbf{L_2}$ are very complicated and rich in signals, particularly at pH>10. Only few of them could be assigned to the non-labile protons of $\mathbf{L_1}$ and $\mathbf{L_2}$. In the ^{1}H NMR spectra of $\mathbf{L_1}$ the aryl protons (*a*, *b*, *c*), the benzylic protons (*d*), the methylene protons of the phosphonate group (*e*), the methyne proton of the pendant arm (*f*) and the methylene

protons of the acetate groups (*g, h*) attached to the ring nitrogens give rise to three resolved multiplets (*a*, *b*, *c*), two AB doublets (*d*, *e*, *g*, *h*) and broad multiplet (*f*). In the ^{1}H NMR spectra of $\mathbf{L_2}$ the signals of the aryl protons (*a*, *b*, *c*), the methyne (*d*, *f*) and methylene (*g*, *e*) protons of the pendant arm are six broad multiplets. In this pH range, the partially protonated ligand and the Na^+ complex are present and the exchange between $Na\mathbf{L_{1,2}}$ and $\mathbf{L_{1,2}}^{5-}$ might results in the broad multiplets in the ^{1}H NMR spectra.

Starting from the basic side, the addition of one equivalent of acid to $\mathbf{L_{1,2}}^{5-}$ results in a significant downfield shift of the ^{1}H NMR signals of *a*, *b*, *c*, *d* and *e* protons and the upfield shift of the ^{31}P NMR signal of the phosphonate group of $\mathbf{L_{1,2}}^{5-}$ indicating that the first protonation takes place at the tertiary and secondary nitrogen atoms of the pendant arm of $\mathbf{L_1}^{5-}$ and $\mathbf{L_2}^{5-}$ ligands, respectively. In the pH range 10.5 – 7.5, the signals of the *f*, *g* and *h* methyne and methylene protons are mainly affected by the second and third protonation processes, which occur at at two opposite ring nitrogen atoms possessed by carboxylate function groups. Further lowering of pH resulted in the downfield shift of the ^{1}H NMR signals of *a*, *b*, *c*, *d* and *e* protons and the ^{31}P NMR signal of the phosphonate group between pH 4.0 – 6.5, confirming that the $\log K_4^{H}$ is related to the protonation of the phosphonate groups in the pendant. Finally, the fifth, the sixth and the seventh protonation steps take place at the carboxylate groups of the acetic arms attached to the ring nitrogen atoms and the phosphonate group of the pendant arm, respectively. The $\log K_i^{H}$ values (Table S1) obtained from the ^{1}H-NMR study agree well with the data determined by pH-potentiometry. Comparison of the protonation constants of $\mathbf{L_1}$ and $\mathbf{L_2}$ indicates that the $\log K_1^{H}$ value of $\mathbf{L_1}$ is somewhat lower than that of $\mathbf{L_2}$, whereas its $\log K_2^{H}$ – $\log K_7^{H}$ values are comparable with those of the related $\log K_i^{H}$ values of $\mathbf{L_2}$. The lower $\log K_1^{H}$ protonation constant of the $\mathbf{L_1}$ might be explained by the electron withdrawing effect of the benzyl group attached to the amino nitrogen of the pendant. On the other hand, $\log K_2^{H}$, $\log K_3^{H}$, $\log K_5^{H}$ and $\log K_6^{H}$ value of $\mathbf{L_1}$ and $\mathbf{L_2}$ values are comparable with those of the related $\log K_i^{H}$ values of **HPA-DO3A** obtained at similar condition (0.1 M NaCl, 25°C).

II.2. Complexation properties of L_1 and L_2

The stability and protonation constants of Ca^{II}, Zn^{II}, Cu^{II} and Gd^{III} complexes of $\mathbf{L_1}$ and $\mathbf{L_2}$, defined by Eqs. (S3) and (S4), were investigated by pH-potentiometry and spectrophotometry at 25 ºC in 0.15 M NaCl solution.

$$K_{ML} = \frac{[ML]}{[M][L]} \qquad (S3)$$

$$K_{MH_iL} = \frac{[MH_iL]}{[MH_{i-1}L][H^+]} \quad (S4)$$

$$K_{MLH_{-1}} = \frac{[ML]}{[MLH_{-1}][H^+]} \quad (S5)$$

where i=0, 1, 2, 3. The K_{ML} and K_{MHiL} values characterizing the formation Ca^{II}, Zn^{II}, Cu^{II} and Gd^{III} with $\mathbf{L_1}$ and $\mathbf{L_2}$ have been calculated from the pH-potentiometric titration data obtained at 1:1 metal to ligand concentration ratios. In calculating the equilibrium constants, the best fitting of the mL NaOH – pH data has been obtained by assuming the formation of ML, MHL, MH_2L, MH_3L, MH_4L, MH_5L and MLH_{-1} complexes. The formation of the deprotonated $[M(L_{1,2})H_{-1}]^{n-}$ complexes takes place at pH>8.5 (Eq. (S5)), as indicated by the base consumption in the titration curves (M=Gd^{III}, n=1; Ca^{II}, Zn^{II} and Cu^{II}, n=2). This deprotonation occurs on the alcoholic -OH group.

The stability constant of Gd^{III} complexes formed with $\mathbf{L_1}$ and $\mathbf{L_2}$ has been determined by the "out-of-cell" technique because of the slow complex formation. Usually the formation of **DOTA** and **DOTA** derivative complexes of Ln^{III}-ion in the pH range 2 – 6 takes place via the formation of a diprotonated intermediate complex (e.g. *Ln(H_2**DOTA)**). Structural studies reveal that the carboxylate groups are coordinated to the Ln^{3+} ion and two opposite ring nitrogens are protonated in the intermeduate *Ln(H_2**DOTA**) complex.[S6-S9] The formation of Ln(**DOTA**)$^-$ and their derivative complexes occurs by the slow deprotonation of the intermediate complex (the rate determining step is the loss of the last proton) and by the consequential transformation to the final "in-cage" complex. In the equilibrium systems, the presence of the intermediate, the free Ln^{III} ion and the final Ln(**DOTA**)$^-$ complex should also be taken into account.[S5,S10] The formation and stability constant of the intermediate is expressed by Eqs (S6) and (S7).

$$Ln^{3+} + H_iL \rightleftharpoons *Ln(H_iL) \quad (S6)$$

$$^*K_{Ln(H_iL)} = \frac{[Ln(H_iL)]}{[Ln^{3+}][H_iL]} \quad (S7)$$

where *i*=2 for the formation of the Ln(DOTA) complexes, but *i*=4 for the formation of Ln$\mathbf{L_1}$ and Ln$\mathbf{L_2}$ because of the presence of the protonated remote amino nitrogen atom and phosphonate group, which are not affected by the formation of the "out-of-cage" complex. The "out-of-cage" complexes are formed rapidly, so their stability constants have been

determined by direct pH-potentiometric titration of Gd^{III}-**L_1** and Gd^{III}-L_2 systems at 1:1 metal to ligand concentration ratios in the pH range 1.7 – 4.0. In the "out-of-cell" samples the measured equilibrium pH values were between 2.5 - 4.0. At such relatively low pH values the amino nitrogen atom and one of the phosphonate -OH group of the pendant is protonated, so for Gd**L_1** and Gd**L_2** complexes the stability constant of the diprotonated complex ($\log\beta_{GdH2L}=[GdH_2L]/[Gd^{3+}][L][H^+]^2$) could be determined. By the calculation of the stability constants in Gd^{3+}-**L_1** and Gd^{3+}-**L_2** systems the presence of Gd^{III} ions, *Gd(H_4L) intermediates and GdH_2L complexes were assumed. For the complete characterization of the complexation in Gd^{III}-**L_1** and Gd^{III}-**L_2** systems, the protonated GdH_2L complexes (which are completely formed at about pH=4.0), have been titrated in the pH range 4.0 – 12.5. During these titrations, base consumption processes have been observed at about pH>4.0, pH, which indicated the deprotonation of the $GdH_2L_{1,2}$ complexes by the formation of GdHL, GdL and $GdLH_{-1}$ species via the dissociation of H^+ ion from the phosphonate –OH, amino NH^+ and alcoholic –OH groups, respectively. The stability constant of the diprotonated Gd(H_2**L_1**) and Gd(H_2**L_2**) has also been determined by measuring the relaxivities of equilibrium solutions ([Gd^{III}]=[**$L_{1,2}$**]=0.002 M) in separate samples (out-of-cell method) in the pH range 2.5 – 4.0. At higher pH values (4.5<pH<12.5) the relaxivities could be measured by direct titration of the samples. The data are presented in Figure S3. The relaxivities of Gd_{aq}^{III}, "out-of-cage" *Gd(H_4**$L_{1,2}$**), the diprotonated Gd(H_2**$L_{1,2}$**) and the monoprotonated Gd(H**$L_{1,2}$**) complexes are shown in Table S2. The stability constant of Gd**L_1** and Gd**L_2** complexes has been calculated by fitting the measured relaxation rates to the Eq. (S8).

$$r_{lobs} = r_1^{w} + r_1^{Gd}[Gd^{3+}] + r_1^{*Gd(H_4L)}[*Gd(H_4L)] + r_1^{GdH_2L}[GdH_2L] \qquad (S8)$$

where r_1^w=0.38 s^{-1}, r_1^{Gd}=13.12 $mM^{-1}s^{-1}$, $r_1^{*Gd(H_4L)}$, $r_1^{GdH_2L}$ and r_1^{GdHL} are the relaxivity values of the H_2O, Gd_{aq}^{3+}, *Gd(H_4L) intermediate and the diprotonated Gd(H_2L) complexes, respectively. By expressing the concentration of the different species by the stability ($\log\beta_{Gd(H2L1,2)}$) and the protonation constants ($\log K_{Gd(HL1,2)}$, $\log K_{Gd(H2L1,2)}$), the stability constant ($\log K_{GdL1,2}$) of Gd**L_1** and Gd**L_2** complexes could be calculated.

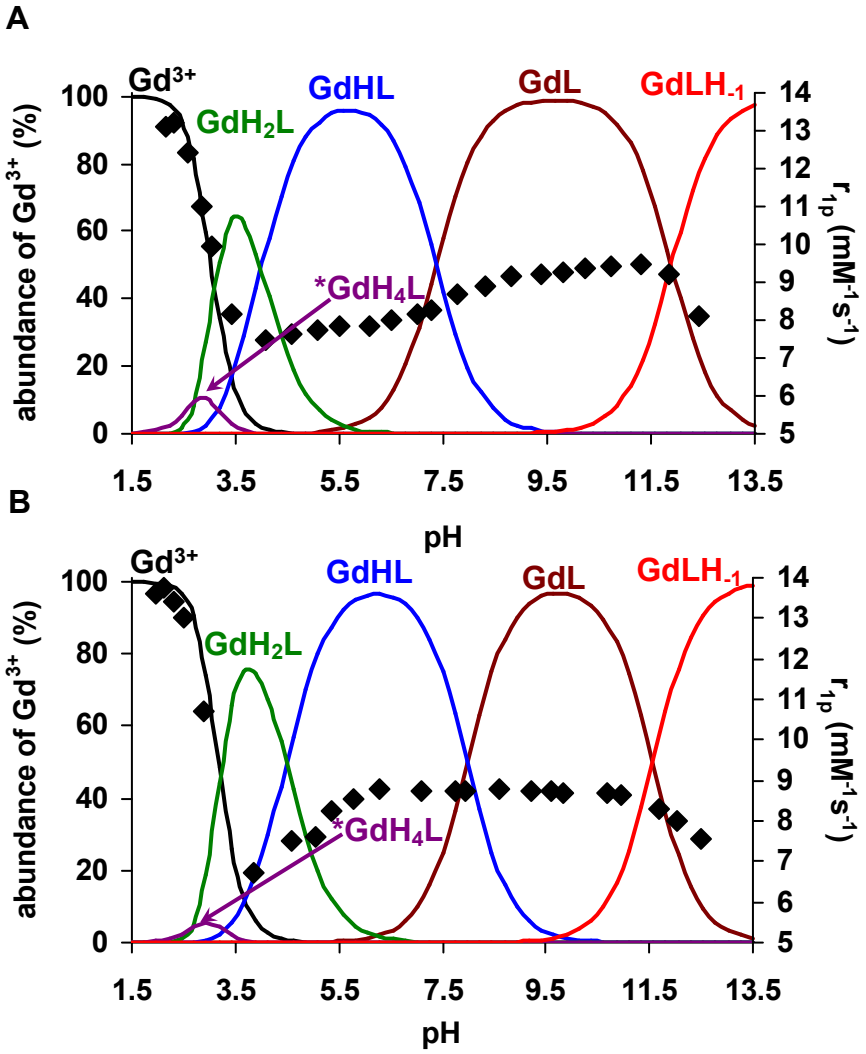

Figure S3. Species distribution and the relaxivity values of the Gd^{III}-$\mathbf{L_1}$ (**A**) and Gd^{III}-$\mathbf{L_2}$ (**B**) systems. ([Gd^{3+}]=[$\mathbf{L_1}$]= [$\mathbf{L_2}$]=1.0 mM, 20 MHz, 0.15 M NaCl, 25°C)

Table S2. Relaxivity values of GdH_2L complexes ($r_1^{GdH_2L}$) and *Gd(H_4L) intermediates ($r_1^{*Gd(H_4L)}$) at 20 MHz (0.15 M NaCl, 25°C):

	$\mathbf{GdL_1}$	$\mathbf{GdL_2}$
$r_1^{GdH_2L}$ ($mM^{-1}s^{-1}$)	6.00 (4)	6.10 (5)
$r_1^{*Gd(H_4L)}$ ($mM^{-1}s^{-1}$)	24.42 (3)	24.74 (4)

The $r_1^{*Gd(H_4L)}$ values were determined by measuring the r_{1obs} values of the samples as a function of time and it was extrapolated to t=0 time. (1 mM Gd^{III} + 10 mM ligand, [NMP]=0.01 M, pH=4.0, 20 MHz, 0.15 M NaCl, 25°C).

The stability and protonation constants of Cu$\mathbf{L_1}$ and Cu$\mathbf{L_2}$ complexes have also determined by spectrophotometry. The equilibrium reaction (Eq. (S9)) has been studied in the [H^+] range of 0.01 – 1.0 M (I=[Na^+]+[H^+]=0.15, [H^+]≤0.15 M), where the formation of Cu^{II}, CuH_4L, CuH_5L

and H_xL species was assumed (x=6 and 7; y=1, 2 and 3). Some characteristic absorption spectra are shown in Figure S4.

$$Cu^{2+} + H_xL \rightleftharpoons [Cu(H_{x-y}L)] + yH^+ \qquad (S9)$$

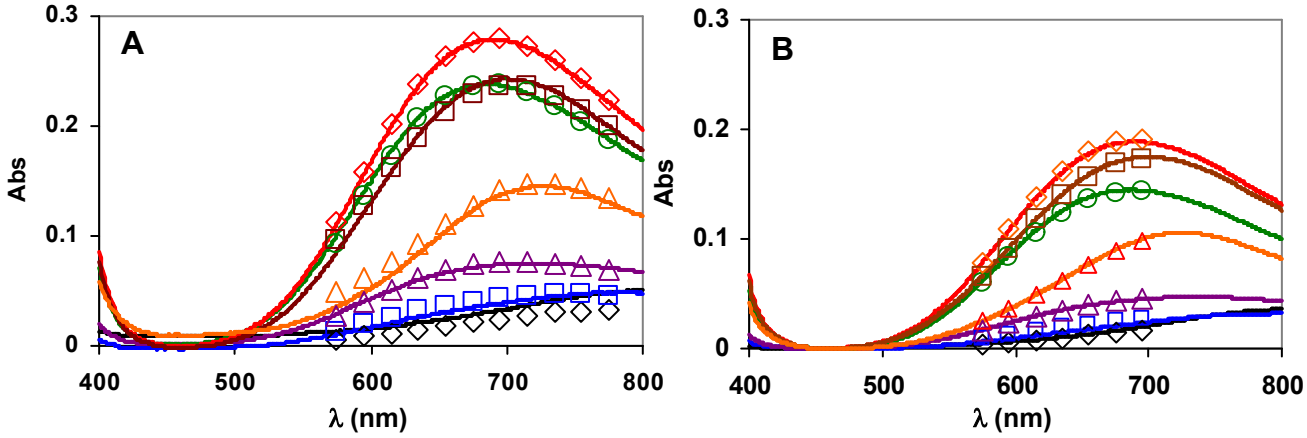

Figure S4. Absorbtion spectra of Cu^{II}–$\mathbf{L_1}$ (**A**) and Cu^{II}–$\mathbf{L_2}$ (**B**) systems. The solid lines and the open symbols represent the experimental and the calculated absorbance values, respectively. (**A**: $[Cu^{2+}]=[\mathbf{L_1}]=2.0$ mM, **B**: $[Cu^{II}]=[\mathbf{L_2}]=1.5$ mM; $[H^+]$ = **1.0**, **0.60**, **0.40**, **0.15**, **0.08**, **0.04** and **0.01** M, l=1 cm, 25 °C, I=$[Na^+]+[H^+]$=0.15 M, $[H^+]\leq 0.15$ M).

The stability and protonation constants of the Ca^{II}-, Zn^{II}-, Cu^{II}- and Gd^{III}-complexes of $\mathbf{L_1}$ and $\mathbf{L_2}$ determined by pH-potentiometry, ^1H NMR relaxometry, spectrophotometry are summarized and compared with those of the corresponding metal complexes formed by **HP-DO3A** and **HPA-DO3A** ligands in Table S3. The comparison of the stability constants reveals that the $\log K_{ML}$ values of the Ca^{II}, Zn^{II}, Cu^{II} and Gd^{III}-complexes formed with $\mathbf{L_1}$ and $\mathbf{L_2}$ are comparable and are about 2 – 4 orders of magnitude lower than those of the corresponding **HP-DO3A** complexes. However, the $\log K_{ML}$ values of L_1, L_2 and **HPA-DO3A** complexes formed with Ca^{II}, Zn^{II} and Gd^{III} ions are very similar. In principle, the determination of the stability constants of metal complexes requires the knowledge of the protonation constants of the ligands. Protonation constants of the free ligands are determined by using constant ionic background (some salts like KCl, NaCl, Me_4NCl, etc.) which has to be selected very carefully because the involved cation can interact with the ligand (i.e. affecting the protonation constant) and the anion may form complexes with the metal ion (i.e. affecting the determination of the stability constant). The $\log K_i^H$ and $\log K_{ML}$ values, published in literature were most generally determined in 0.1 M KCl or 0.1 M Me_4NCl solution.[S11] The protonation constants of ligands particularly the $\log K_1^H$ values obtained in 0.15 M NaCl are lower than those determined in 0.1 M KCl or 0.1 M Me_4NCl solutions. The lower $\log K_i^H$

values obtained in NaCl solutions can be interpreted in terms of the interaction between the fully deprotonated ligands and the smaller Na^+ ion, which is stronger than that of the larger K^+ or Me_4N^+ ions. The largest difference between the $\log K_1^H$ values obtained in NaCl and KCl or Me_4NCl solutions has been determined for macrocyclic ligands which form relatively stable complexes with Na^+ ion ($\log K_{Na(\mathbf{DOTA})}$=4.38).[S12]

The stability constant of Gd(**HP-DO3A**) determined in 0.1 M Me_4NCl solution ($\log K_{GdL}$=23.8)[S4] is significantly higher than that of Gd$\mathbf{L_1}$ and Gd$\mathbf{L_2}$ (Table S3) due to the significantly lower basicity of the ring nitrogen atoms of $\mathbf{L_1}$ and $\mathbf{L_2}$ ligands ($\log K_2^H$, Table S1) obtained in 0.15 M NaCl solution (Table S1). However, the $\log K_{GdL}$ values of Gd$\mathbf{L_1}$, Gd$\mathbf{L_2}$ and Gd(**HPA-DO3A**) determined in similar condition are comparable indicating the nearly identical thermodynamic properties of Gd^{III}-complexes formed with $\mathbf{L_1}$, $\mathbf{L_2}$ and **HPA-DO3A**.

The $\log K_{ML}$ values of the Ca^{II}- , Zn^{II}- and Cu^{II}-complexes formed with $\mathbf{L_1}$, $\mathbf{L_2}$ and **HPA-DO3A** are also comparable which might be explained by the similar coordination environment of Ca^{II}, Zn^{II} and Cu^{II} ions in these complexes. On the other hand, the presence of the pendant groups in $\mathbf{L_1}$ and $\mathbf{L_2}$ does not alter the stability constant of the Ca^{II}-, Zn^{II}- and Cu^{II}-complexes, which indicates that the remote donor atoms of the pendant arms of L_1, L_2 and **HPA-DO3A** ligands do not take place in the coordination of the Ca^{II}, Zn^{II} and Cu^{II} ions.

The comparison of the $\log K_{MHiL}$ values of the Ca^{II}-, Zn^{II}- and Cu^{II}-complexes formed with $\mathbf{L_1}$ and $\mathbf{L_2}$ ligands with those of the corresponding **HP-DO3A** and **HPA-DO3A** complexes (Table S3) reveals that the first and second protonation $CaL_{1,2}$, $ZnL_{1,2}$ and $CuL_{1,2}$ take place on the remote amino N and the basic phosphonate $–O^-$ donor atoms of the pendant arm in $\mathbf{L_1}$ and $\mathbf{L_2}$ ligands, respectively. The $\log K_{MHL}$ and $\log K_{MH2L}$ values of Ca$\mathbf{L_{1,2}}$, Zn$\mathbf{L_{1,2}}$ and Cu$\mathbf{L_{1,2}}$ are somewhat lower than that of the corresponding protonation constants ($\log K_1^H$ and $\log K_4^H$, Table S1) of the free $\mathbf{L_1}$ and $\mathbf{L_2}$ ligands. At lower pH values the further protonations of Ca$\mathbf{L_{1,2}}$, Zn$\mathbf{L_{1,2}}$ and Cu$\mathbf{L_{1,2}}$ take place on the non- or weakly coordination carboxylate groups of the macrocycle and the non-protonated phosphonate $–O^-$ donor atom of the pendant arm.

Table S3. Stability and protonation constants of Ca^{II}-, Zn^{II}-, Cu^{II}- and Gd^{III}- complexes formed with $\mathbf{L_1}$, $\mathbf{L_2}$, **HP-DO3A** and **HPA-DO3A** (25°C):

	$\mathbf{L_1}$	$\mathbf{L_2}$	**HP-DO3A**[a]	**HPA-DO3A**[b]
I	**0.15 M NaCl**		**0.1 M Me_4NCl**	**0.15 M NaCl**
CaL	**11.53 (3)**	**11.14 (4)**	**14.83**	**12.13**
CaHL	**8.67 (2)**	**9.34 (3)**	–	4.67
CaH_2L	**5.43 (3)**	**6.32 (1)**	–	–
ZnL	**16.86 (4)**	**16.94 (3)**	**19.37**	**17.18**
ZnHL	**8.71 (2)**	**9.42 (5)**	3.7	3.67
ZnH_2L	**5.23 (2)**	**5.94 (4)**	–	2.87
ZnH_3L	3.65 (3)	3.78 (5)	–	–
ZnH_4L	3.49 (1)	3.51 (2)	–	–
****CuL**	**20.99 (7)**	**20.49 (1)**	**22.84**	**21.53**
CuHL	**8.85 (2)**	**9.21 (4)**	3.72	4.00
CuH_2L	**5.26 (2)**	**5.59 (5)**	2.3	1.24
CuH_3L	3.96 (4)	3.86 (5)	–	–
CuH_4L	2.01 (4)	2.03 (4)	–	–
CuH_5L	1.66 (5)	1.50 (5)	–	–
GdL **Relax.**	**19.93 (7)**	**19.16 (9)**	**23.8**	**18.41**
pH-pot.	**20.25 (4)**	**19.66 (8)**		
GdHL	**7.36 (1)**	**7.98 (3)**	–	–
GdH_2L	**4.00 (2)**	**4.49 (4)**	–	–
$GdLH_{-1}$	**12.31 (1)**	**11.56 (2)**	**11.31**[c]	**6.73**
*GdH_4L	5.10 (2)	5.05 (4)	5.10[b] (*GdH_2L)	5.72[b] (*GdH_2L)

[a] Ref. [S4]; [b] Ref. [S5], [c] Ref. [S13] 0.15 M NaCl, 25°C; * stability constants of the protonated *Gd(H_2L) out-of-cage complex (intermediate) *$K_{Gd(HiL)}$=[Gd(H_2L)]/[Gd^{3+}][H_2L].

On the other hand, the first and second protonation constants particularly the logK_{MHL} value (Table S3) of Gd$\mathbf{L_1}$ and Gd$\mathbf{L_2}$ complexes are significantly smaller than logK_1^H and logK_4^H values of the free $\mathbf{L_1}$ and $\mathbf{L_2}$ ligands. Since the remote basic phoshonate $-O^-$ and the amino N donor atoms are not coordinated to Gd^{III}-ion, the lower logK_{MHL} and logK_{MH2L} values of the Gd$\mathbf{L_{1,2}}$ complexes might be explained by the electrostatic repulsion between the Gd^{III}-coordinated –OH group and the protonated basic phosphonate –OH and amino NH^+ moieties of the pendant arm. Interestingly, the protonation constant of –OH group (logK_{GdLH-1}) of Gd$\mathbf{L_2}$ complex is comparable, whereas the logK_{GdLH-1} value of Gd$\mathbf{L_1}$ is significantly higher than that of the Gd(**HP-DO3A**). The deprotonation of the –OH group in Gd(**HPA-DO3A**) is

characterized by significantly smaller logK_{GdLH-1} value due to the presence of the strong electron withdrawing amide group on the hydroxyl-ethyl pendant arm.[S5] In order to explain the protonation behaviour of –OH group in Gd(**HP-DO3A**) derivatives, the possible interactions between the coordinated –OH group and the deprotonated basic phosphonate $–O^-$ and amino N donor atoms of Gd$\mathbf{L_{1,2}}$ complexes must be considered in terms of *i)* H-bonding interaction between the -OH group and the deprotonated basic phosphonate $–O^-$ and amino N donor atoms, which might increase the logK_{GdLH-1} value, *ii)* the electrostatic repulsion between the –OH group and the –NH proton of secondary amino nitrogen of the pendant which reduces the logK_{GdLH-1} value of Gd$\mathbf{L_2}$ and *iii)* the electron withdrawing effect of the aromatic substituent, which decreases the logK_{GdLH-1} value. The combined effect of these processes might be responsible for the different protonation constants of the –OH group of Gd$\mathbf{L_1}$ and Gd$\mathbf{L_2}$ complexes by comparing with that of the Gd(**HP-DO3A**). Specifically, the higher logK_{GdLH-1} value of Gd$\mathbf{L_1}$ might be explained by the strong H-bond formation of the –OH group with the basic phosphonate $–O^-$ and the tertiary amino N donor atoms of the pendant arm. The electrostatic repulsion between –OH group and the proton of the secondary –NH moiety of the pendant can explain the lower logK_{GdLH-1} value of Gd$\mathbf{L_2}$ complex.

III. Kinetic inertness of Gd$\mathbf{L_1}$ and Gd$\mathbf{L_2}$ complexes.

The rates of dissociation of the Gd^{III} complexes formed with the **HP-DO3A** derivatives are slow processes. Since the dissociation of macrocyclic Gd^{III} complexes generally occurs through proton assisted pathway,[S5,S6,S10,S14-S16] the studies on the rates of dissociation have been performed in 0.01 – 1.0 M HCl solution ($[H^+]<0.15$ M, $[H^+]+[Na^+]=0.15$ M NaCl, 25°C). According to the equilibrium studies the Gd$\mathbf{L_1}$ and Gd$\mathbf{L_2}$ complexes dissociate completely at $[H^+]>0.01$ M. In 0.01 M HCl solution a few percent Gd^{III} complex in equilibrium would be present, but with the study of the first 50% of the dissociation reaction the effect of the remainder Gd^{III} complex is negligible. The relaxation effect of the released free Gd^{III} ion is significantly higher than that of the Gd^{III} complexes, so the rates of dissociation could be studied by measuring the relaxation rates of water protons. In the presence of HCl excess, the decomplexation of Gd$\mathbf{L_1}$ and Gd$\mathbf{L_2}$ can be treated as a pseudo-first-order process and the reaction rate can be expressed by Eq. (S10), where k_d is a pseudo-first-order rate constant, $[GdL]_t$ and $[GdL]_{tot}$ are the concentrations of the GdL species at time *t* and the total concentration of the complex, respectively.

$$-\frac{d[GdL]_t}{dt} = k_d[GdL]_{tot} \qquad (S10)$$

The rates of the transmetallation reactions have been studied at different concentrations of the HCl ([HCl]=0.01 – 1.0 M, 25°C). The k_d values as a function of $[H^+]$ are shown in Figure S5.

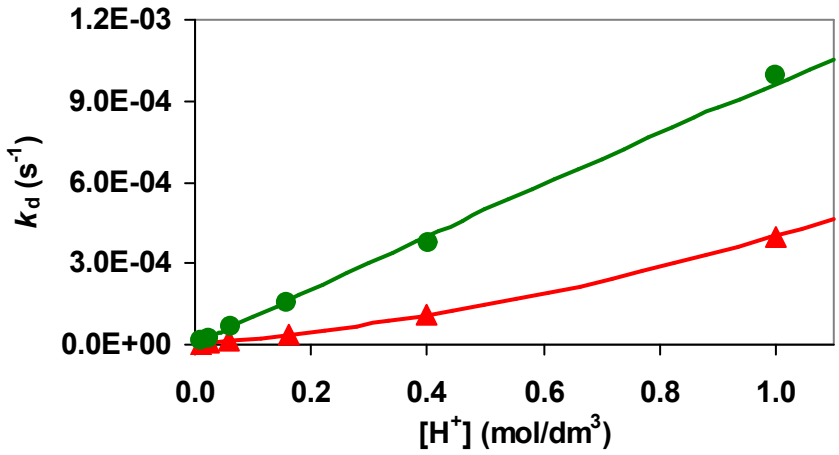

Figure S5. Pseudo-first-order rate constant (k_d) characterizes the dissociation of Gd**L**$_1$ (ᘐ) and Gd**L**$_2$ (□) as a function of $[H^+]$. The solid lines and the symbols represent the experimental and the calculated k_d values ([Gd**L**$_1$]=[Gd**L**$_2$]=1.0 mM, $[H^+]\leq 0.15$ M→$[Na^+]+[H^+]=0.15$ M, 25°C).

The obtained k_d pseudo-first order rate constants are directly proportional to the concentration of H^+. To interpret the direct proportionality between the H^+ ion concentration and the k_d rates characterize the dissociation of GdL_1 and GdL_2 complexes further protonation of the GdH_2L species (dominates at pH about 2) have to assume. The formation of the GdH_3L species is probably occurs rapidly in equilibrium reactions, characterized by the protonation constant K_{GdH3L}.

$$GdH_2L + H^+ \overset{K_{GdH_3L}}{\rightleftharpoons} GdH_3L \qquad (S11)$$

$$K_{GdH_3L} = \frac{[GdH_3L]}{[GdH_2L][H^+]}$$

The dissociation of the species GdH_3L may take place spontaneously:

$$GdH_3L \xrightarrow{k_{GdH_3L}} Gd^{3+} + H_3L \qquad (S12)$$

where k_{GdH3L} is the rate constants characterizing the spontaneous dissociation of the protonated GdH_3L species. However, the k_d values of Gd**L**$_2$ complex obtained at $[H^+]>0.16$ M indicate that dissociation might take place with the attack of a second H^+ ion on the GdH_3L species (k^H_{GdH3L}).

$$GdH_3L + H^+ \xrightarrow{k^H_{GdH_3L}} Gd^{3+} + H_4L \qquad (S13)$$

By considering all the possible pathways and the rate of dissociation of Gd**L$_1$** and Gd**L$_2$** complexes (Eq. (S10)), the pseudo-first-order rate constant (k_d) can be expressed by Eq. (S14).

$$-\frac{d[\mathrm{GdL}]_t}{dt} = k_d[\mathrm{GdL}]_t = k_{\mathrm{GdH_3L}}[\mathrm{GdH_3L}] + k^{\mathrm{H}}_{\mathrm{GdH_3L}}[\mathrm{GdH_3L}][\mathrm{H^+}] \qquad (S14)$$

By taking into account the total concentration of the complex ($[GdL]_t=[GdH_2L]+[GdH_3L]$), the protonation constants of the GdH_2L species (K_{GdH3L}, Eq. (S11)) and Eq. (S14), the pseudo-first-order rate constant (k_d) can be expressed as follows:

$$k_d = \frac{k_1[\mathrm{H^+}] + k_2[\mathrm{H^+}]^2}{1 + K_{\mathrm{GdH_{n+1}L}}[\mathrm{H^+}]} \qquad (S15)$$

where $k_1 = k_{GdH3L} \times K_{GdH3L}$ and $k_1 = k^{H}_{GdH3L} \times K_{GdH3L}$ are the rate constants characterizing the spontaneous and proton-assisted dissociation of GdH_3L species formed by Gd**L$_1$** and Gd**L$_2$** complexes. The protonation constant (K_{GdHL}) of Gd(**DOTA**)-like complexes are relatively small (Gd(**DOTA**): K_{GdHL} =14).[S6] However, the protonation process could not be detected in the pH-potentiometric studies of Gd**L$_1$** and Gd**L$_2$** complexes at pH<3. By taking into account the very low protonation constant of Gd**L$_1$** and Gd**L$_2$** complexes (K_{GdH3L}<<10), the denominator of Eq. (S15) (1>> K^{H}_{GdHL} [H$^+$]) can be neglected, so Eq. (S15) can be simplified in the form of Eq. (S16). The k_1 and k_2 values have been calculated by fitting of the kinetic data (Figure S5) to Eq. (S16). The last term of Eq. (S16) has been neglected in the calculation of the kinetic parameters characterizing the dissociation of the Gd**L$_1$** complex.

$$k_d = k_1[\mathrm{H^+}] + k_2[\mathrm{H^+}]^2 \qquad (S16)$$

III. Interaction of GdL_1 and GdL_2 with HSA

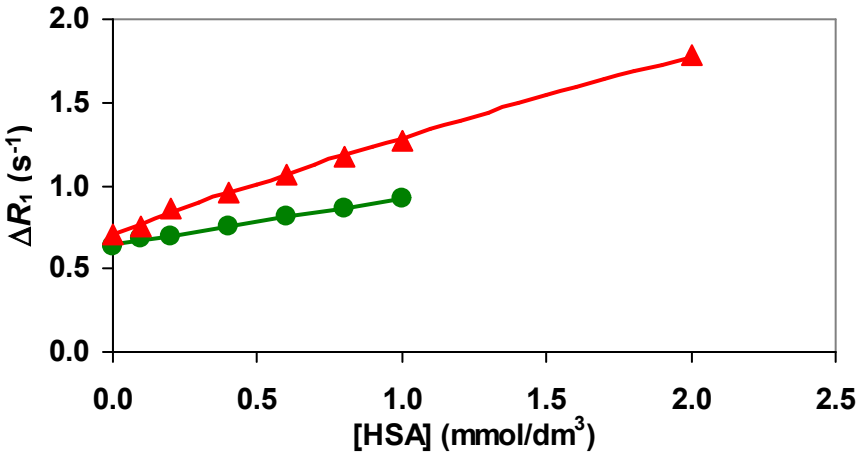

Figure S6. Water proton relaxation rate (R_1) of Gd**L**$_1$ (ᔓ) and Gd**L**$_2$ (□) complexes as a function of [HSA]. ([Gd**L**$_1$]=0.090 mM, [Gd**L**$_2$]=0.085 mM, pH=7.4, 20 MHz, 310 K).

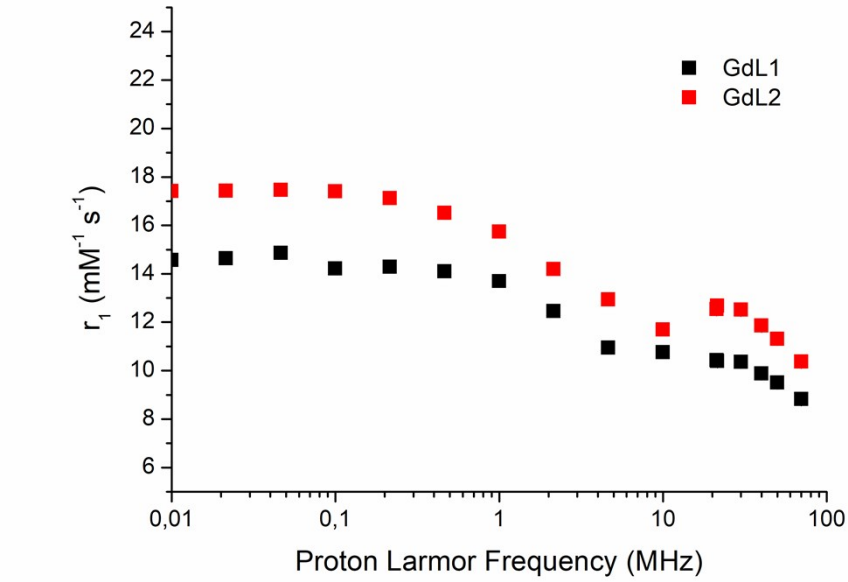

Figure S7. NMRD profile of Gd**L**$_1$ and Gd**L**$_2$ in the presence of human plasma ([Gd**L**$_1$]=[Gd**L**$_2$]=1.0 mM, pH=7.4, 37°C)

V. X-Ray diffractions studies of $\{(C(NH_2)_3)[LuL_1(H_2O)]\}\cdot 3H_2O$

The colorless Lu**L**$_1$ complex was crystallized the slow diffusion of EtOH and Et_2O mixture to aqueous solution of Lu^{III}-complex prepared from equimolar $Lu(OH)_3$ and racemic H_5**L**$_1$, the pH was adjusted to pH=9 using guanidinium carbonate. Several crystals were studied by single crystal X-ray diffraction method. XRD data collection was carried out at 293 K using

Mo-Kα radiation (λ = 0.71073 Å) with a Burker-Nonius MACH3 diffractometer equipped with point detector. Crystallographic and experimental details of the data collection and refinement of the structure of $\{(C(NH_2)_3)[Lu\mathbf{L_1}(H_2O)]\}\cdot 3H_2O$ are reported in Table S4. Unexpectedly, all crystals diffracted rather weakly, even the large volume ones and the peaks were very diffuse, an example is shown at Figure S8. Moreover, crystals were rather easily decomposing under X-ray radiation showing decay of 40%. Even low temperature data collection could not give better results as quality of the crystals were further degraded by cooling and no further batches of crystals could be prepared. Finally, several datasets were collected and even the best one was manipulated. However, after careful integration the structure could be solved by SIR-92 program and refined by full-matrix least-squares method on F^2. Unfortunately, only heavy lutetium and phosphorous atoms could be refined with anisotropic atomic displacement parameters using the SHELX package while the light atoms should be kept isotropic to prevent collapse of the refinement. Fortunately, the atoms and their connectivity of the ligand could be localized, in some cases even hydrogen atoms of solvent water molecules could be found on the difference electron density map and remaining significant peaks very close to the lutetium atom. Distances of hydrogen and oxygen atoms were restrained in the final stage of the refinement and several other RIGU restrains should be applied to regulate thermal parameters of carbon atoms. Altogether hydrogen atoms were treated with a mixture of independent and constrained refinement. Publication material was prepared with the WINGX-suite. Also, especially the water molecules had significant shifts even after prolonged refinement. These features of the structure resulted in high R values, shift, and several ‘A’ and ‘B’ level errors in checkcif report. Nevertheless the overall structure of the complex is sufficient to answer the structural questions i.e. coordination of Lu^{III} and s . All crystallographic data are deposited in the Cambridge Crystallographic Data Centre under CCDC 2042633.

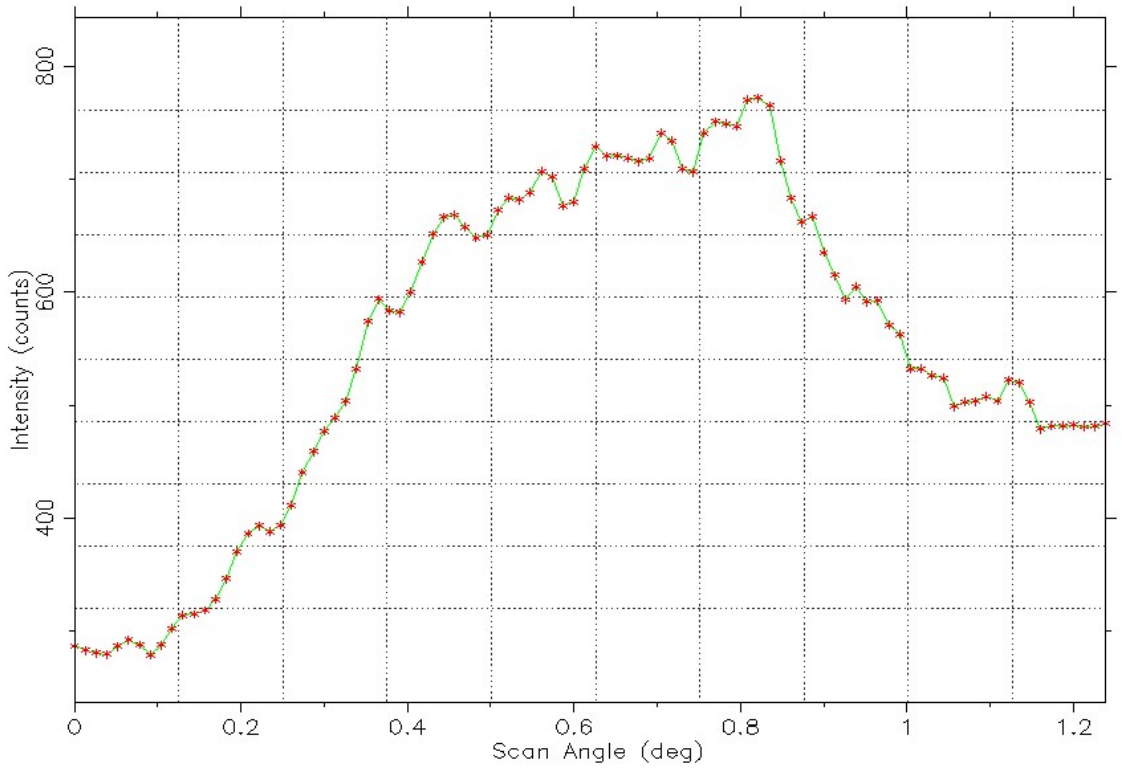

Figure S8. The representative peak profile measured by single crystal X-Ray diffraction.

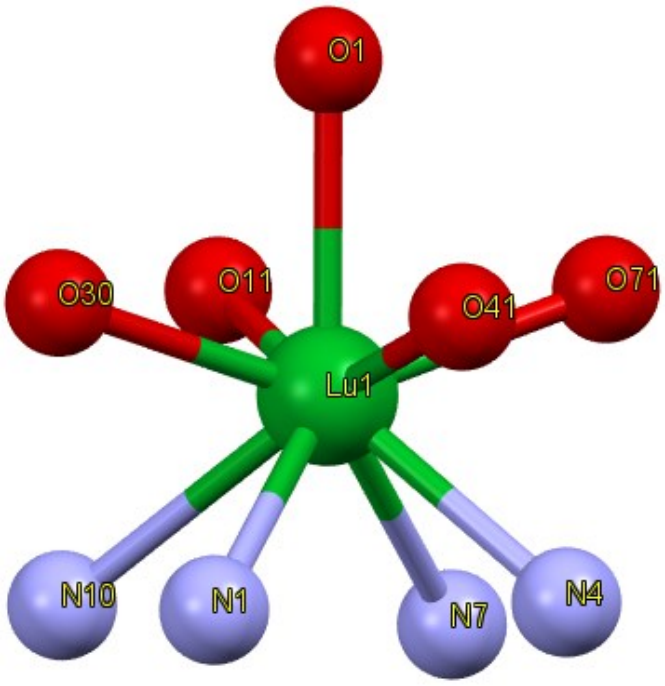

Figure S9. The coordination polyhedron around the Lu^{III} ion in $\{(C(NH_2)_3)_2[Lu\mathbf{L_1}(H_2O)]\}\cdot 3H_2O$

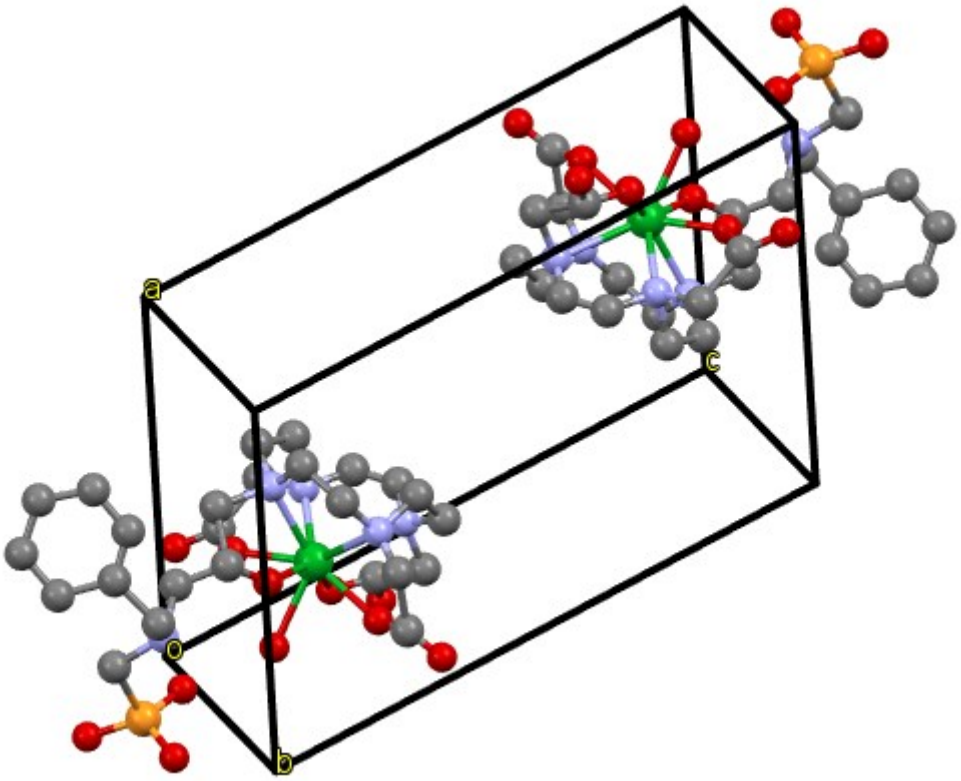

Figure S10. Packing diagram of $\{(C(NH_2)_3)_2[Lu\mathbf{L}_1(H_2O)]\}\cdot 3H_2O$. Hydrogen atoms are omitted for simplicity.

Table S4. Experimental details of X-ray structure determination

Chemical formula	$C_{25}H_{37}LuN_5O_{11}P{\cdot}CH_6N_3{\cdot}3(H_2O)$
M_r	903.67
Crystal system, space group	Triclinic, $P\bar{1}$
Temperature (K)	293
a, b, c (Å)	10.893 (1), 12.941 (1), 15.295 (1)
α, β, γ (°)	88.65 (1), 72.01 (1), 69.87 (1)
V (Å^3)	1917.1 (3)
Z	2
Radiation type	Mo $K\alpha$
μ (mm^{-1})	2.69
Crystal size (mm)	0.4 × 0.25 × 0.2
Data collection	
Diffractometer	Enraf Nonius MACH3
Absorption correction	ψ scan.[S17].Number of ψ scan sets used was 4 Theta correction was applied. Averaged transmission function was used. Fourier smoothing - Window value 5
T_{min}, T_{max}	0.071, 0.960
No. of measured, independent and observed [$I > 2\sigma(I)$] reflections	6511, 6511, 2467
$(\sin\theta/\lambda)_{max}$ (Å^{-1})	0.608
Refinement	
$R[F^2 > 2\sigma(F^2)]$, $wR(F^2)$, S	0.337, 0.619, 2.10
No. of reflections	6511
No. of parameters	230
No. of restraints	29
H-atom treatment	H atoms treated by a mixture of independent and constrained refinement
$(\Delta/\sigma)_{max}$	0.533
$\Delta\rangle_{max}$, $\Delta\rangle_{min}$ (e Å^{-3})	3.57, -6.03

Computer programs: MACH3/PC,[S18] PROFIT,[S19] *SIR92*,[S20] *SHELXL2016*/4,[S21] *ORTEP-3 for Windows* and *WinGX* publication routines[S22]

Table S5. Geometric parameters (Å, º)

C1G—N3G	1.41 (7)	C42—O41	1.34 (10)
C1G—N2G	1.17 (7)	C50—N50	1.501 (11)
C1G—N1G	1.36 (7)	C50—P51	1.9 (2)
C2—N1	1.37 (10)	C50—H50A	0.97
C2—C3	1.501 (10)	C50—H50B	0.97
C2—H2A	0.97	C60—N50	1.44 (6)
C2—H2B	0.97	C60—C61	1.61 (8)
C3—N4	1.20 (9)	C60—H60A	0.97
C3—H3A	0.97	C60—H60B	0.97
C3—H3B	0.97	C61—C62	1.58 (9)
C5—C6	1.501 (10)	C61—C66	1.57 (8)
C5—N4	1.504 (10)	C62—C63	1.28 (9)
C5—H5A	0.97	C62—H62	0.93
C5—H5B	0.97	C63—C64	1.23 (9)
C6—N7	1.498 (10)	C63—H63	0.93
C6—H6A	0.97	C64—C65	1.48 (9)
C6—H6B	0.97	C64—H64	0.93
C8—C9	1.497 (10)	C65—C66	1.33 (9)
C8—N7	1.500 (10)	C65—H65	0.93
C8—H8A	0.97	C66—H66	0.93
C8—H8B	0.97	C71—C72	1.501 (12)
C9—N10	1.499 (10)	C71—N7	1.25 (18)
C9—H9A	0.97	C71—H71A	0.97
C9—H9B	0.97	C71—H71B	0.97
C11—N10	1.502 (10)	C72—O71	0.98 (6)
C11—C12	1.504 (7)	C72—O72	1.65 (7)
C11—H11A	0.97	C72—LU1	2.68 (6)
C11—H11B	0.97	N1—LU1	2.65 (6)
C12—N1	1.502 (10)	N1G—H1G1	0.86
C12—H12A	0.97	N1G—H1G2	0.86
C12—H12B	0.97	N2G—H2G1	0.86
C13—N10	1.43 (8)	N2G—H2G2	0.86
C13—C14	1.60 (11)	N3G—H3G1	0.86
C13—H13A	0.97	N3G—H3G2	0.86
C13—H13B	0.97	N4—LU1	2.89 (6)
C14—O12	1.16 (11)	N7—LU1	2.68 (13)
C14—O11	1.27 (10)	N10—LU1	2.94 (8)
C31—C32	1.32 (9)	O1—LU1	2.29 (4)

C31—N1	1.502 (10)	O1W—H11	0.89 (8)
C31—H31A	0.97	O1W—H12	0.88 (5)
C31—H31B	0.97	O2W—H21	0.87 (9)
C32—O30	1.51 (8)	O2W—H22	0.86 (10)
C32—C33	1.44 (9)	O3W—H31	0.90 (12)
C32—H32A	0.98	O11—LU1	2.31 (4)
C33—N50	1.43 (8)	O30—LU1	2.37 (4)
C33—H33A	0.97	O30—H30	0.93
C33—H33B	0.97	O41—LU1	2.49 (5)
C41—N4	1.54 (7)	O51—P51	1.40 (4)
C41—C42	1.21 (10)	O52—P51	1.73 (6)
C41—H41A	0.97	O53—P51	1.59 (5)
C41—H41B	0.97	O71—LU1	2.18 (4)
C42—O42	1.66 (10)		
Bond angles			
N3G—C1G—N2G	120 (6)	C66—C65—H65	121.6
N3G—C1G—N1G	113 (6)	C64—C65—H65	121.6
N2G—C1G—N1G	126 (6)	C65—C66—C61	120 (7)
N1—C2—C3	74 (7)	C65—C66—H66	120
N1—C2—H2A	116.5	C61—C66—H66	120
C3—C2—H2A	116.6	C72—C71—N7	105 (10)
N1—C2—H2B	115.9	C72—C71—H71A	111.9
C3—C2—H2B	115.6	N7—C71—H71A	112.9
H2A—C2—H2B	113.1	C72—C71—H71B	109
C2—C3—N4	149 (10)	N7—C71—H71B	108.7
C2—C3—H3A	99.9	H71A—C71—H71B	108.9
N4—C3—H3A	99.9	O71—C72—O72	110 (6)
C2—C3—H3B	99	O71—C72—C71	140 (10)
N4—C3—H3B	98.9	O72—C72—C71	105 (8)
H3A—C3—H3B	104.1	O71—C72—LU1	50 (4)
C6—C5—N4	106 (5)	O72—C72—LU1	159 (4)
C6—C5—H5A	110.1	C71—C72—LU1	95 (7)
N4—C5—H5A	110.2	C2—N1—C12	95 (5)
C6—C5—H5B	111.1	C2—N1—C31	112 (6)
N4—C5—H5B	110.4	C12—N1—C31	119 (5)
H5A—C5—H5B	108.6	C2—N1—LU1	125 (5)
C5—C6—N7	116 (7)	C12—N1—LU1	118 (3)
C5—C6—H6A	108.4	C31—N1—LU1	90 (4)
N7—C6—H6A	109	C1G—N1G—H1G1	119.9
C5—C6—H6B	108	C1G—N1G—H1G2	120.1

N7—C6—H6B	108	H1G1—N1G—H1G2	120
H6A—C6—H6B	107.5	C1G—N2G—H2G1	120
C9—C8—N7	109 (8)	C1G—N2G—H2G2	120
C9—C8—H8A	109.8	H2G1—N2G—H2G2	120
N7—C8—H8A	109.4	C1G—N3G—H3G1	120.3
C9—C8—H8B	109.9	C1G—N3G—H3G2	119.7
N7—C8—H8B	110	H3G1—N3G—H3G2	120
H8A—C8—H8B	108.2	C5—N4—C41	99 (4)
N10—C9—C8	118 (5)	C5—N4—C3	152 (8)
N10—C9—H9A	107.1	C41—N4—C3	106 (7)
C8—C9—H9A	107.9	C5—N4—LU1	98 (5)
N10—C9—H9B	108	C41—N4—LU1	95 (4)
C8—C9—H9B	108.2	C3—N4—LU1	67 (6)
H9A—C9—H9B	107.3	C6—N7—C8	114 (7)
N10—C11—C12	129 (5)	C6—N7—C71	103 (10)
N10—C11—H11A	104.3	C8—N7—C71	118 (10)
C12—C11—H11A	105.3	C6—N7—LU1	110 (7)
N10—C11—H11B	105.1	C8—N7—LU1	108 (7)
C12—C11—H11B	105.4	C71—N7—LU1	102 (7)
H11A—C11—H11B	106	C13—N10—C11	140 (5)
N1—C12—C11	106 (4)	C13—N10—C9	121 (5)
N1—C12—H12A	110.8	C11—N10—C9	95 (4)
C11—C12—H12A	110.2	C13—N10—LU1	95 (4)
N1—C12—H12B	110.6	C11—N10—LU1	99 (4)
C11—C12—H12B	110.4	C9—N10—LU1	91 (4)
H12A—C12—H12B	108.6	C60—N50—C50	104 (10)
N10—C13—C14	116 (7)	C60—N50—C33	134 (6)
N10—C13—H13A	108.4	C50—N50—C33	111 (10)
C14—C13—H13A	108.5	H11—O1W—H12	149 (10)
N10—C13—H13B	107.7	H21—O2W—H22	152 (10)
C14—C13—H13B	108.5	C14—O11—LU1	124 (6)
H13A—C13—H13B	107.6	C32—O30—LU1	130 (4)
O12—C14—O11	118 (10)	C32—O30—H30	114.9
O12—C14—C13	104 (9)	LU1—O30—H30	114.8
O11—C14—C13	112 (8)	C42—O41—LU1	108 (5)
C32—C31—N1	140 (7)	C72—O71—LU1	110 (4)
C32—C31—H31A	102.1	O52—P51—O53	115 (3)
N1—C31—H31A	102	O52—P51—O51	108 (3)
C32—C31—H31B	102.1	O53—P51—O51	115 (3)
N1—C31—H31B	102.1	O52—P51—C50	105 (10)

H31A—C31—H31B	104.8	O53—P51—C50	107 (6)
O30—C32—C33	101 (6)	O51—P51—C50	106 (8)
O30—C32—C31	89 (6)	O41—LU1—O11	141.1 (16)
C33—C32—C31	109 (7)	O41—LU1—O71	79.5 (15)
O30—C32—H32A	117.7	O11—LU1—O71	88.1 (14)
C33—C32—H32A	117.7	O41—LU1—O30	84.6 (14)
C31—C32—H32A	117.9	O11—LU1—O30	88.6 (14)
C32—C33—N50	107 (6)	O71—LU1—O30	150.0 (14)
C32—C33—H33A	110.2	O41—LU1—N4	69.3 (16)
N50—C33—H33A	110.4	O11—LU1—N4	140.4 (15)
C32—C33—H33B	110.3	O71—LU1—N4	71.3 (16)
N50—C33—H33B	110.2	O30—LU1—N4	125.8 (15)
H33A—C33—H33B	108.6	O41—LU1—O1	73.7 (15)
N4—C41—C42	121 (7)	O11—LU1—O1	67.7 (13)
N4—C41—H41A	107	O71—LU1—O1	77.2 (13)
C42—C41—H41A	107.5	O30—LU1—O1	74.0 (12)
N4—C41—H41B	106.9	N4—LU1—O1	134.7 (13)
C42—C41—H41B	106.9	O41—LU1—N1	76.4 (15)
H41A—C41—H41B	106.8	O11—LU1—N1	134.1 (14)
O42—C42—O41	77 (6)	O71—LU1—N1	133.0 (16)
O42—C42—C41	140 (8)	O30—LU1—N1	65.6 (15)
O41—C42—C41	138 (9)	N4—LU1—N1	62.6 (15)
N50—C50—P51	123 (10)	O1—LU1—N1	131.3 (13)
N50—C50—H50A	106.7	O41—LU1—N7	129.8 (18)
P51—C50—H50A	106.6	O11—LU1—N7	74 (2)
N50—C50—H50B	106.6	O71—LU1—N7	65 (2)
P51—C50—H50B	106.3	O30—LU1—N7	142 (2)
H50A—C50—H50B	106.4	N4—LU1—N7	67 (2)
N50—C60—C61	98 (4)	O1—LU1—N7	126 (3)
N50—C60—H60A	111.9	N1—LU1—N7	103 (3)
C61—C60—H60A	111.9	O41—LU1—N10	142.6 (15)
N50—C60—H60B	112.4	O11—LU1—N10	68.0 (14)
C61—C60—H60B	112.2	O71—LU1—N10	133.9 (14)
H60A—C60—H60B	109.7	O30—LU1—N10	71.1 (12)
C62—C61—C66	116 (6)	N4—LU1—N10	102.2 (14)
C62—C61—C60	119 (5)	O1—LU1—N10	123.1 (12)
C66—C61—C60	125 (5)	N1—LU1—N10	67.9 (13)
C61—C62—C63	104 (7)	N7—LU1—N10	71 (2)
C61—C62—H62	128	O41—LU1—C72	99.4 (17)
C63—C62—H62	128.2	O11—LU1—C72	73.5 (17)

C62—C63—C64	144 (9)	O71—LU1—C72	20.0 (14)
C62—C63—H63	108	O30—LU1—C72	156.2 (17)
C64—C63—H63	108	N4—LU1—C72	76.8 (18)
C63—C64—C65	114 (9)	O1—LU1—C72	84.6 (16)
C63—C64—H64	122.9	N1—LU1—C72	138.2 (19)
C65—C64—H64	122.7	N7—LU1—C72	48 (3)
C66—C65—C64	117 (7)	N10—LU1—C72	114.4 (16)
Torsion angles			
N1—C2—C3—N4	16E1 (2)	C42—C41—N4—C3	-38 (12)
N4—C5—C6—N7	73 (11)	C42—C41—N4—LU1	30 (9)
N7—C8—C9—N10	84 (8)	C2—C3—N4—C5	151 (17)
N10—C11—C12—N1	56 (7)	C2—C3—N4—C41	-6E1 (2)
N10—C13—C14—O12	170 (8)	C2—C3—N4—LU1	-15E1 (2)
N10—C13—C14—O11	-61 (11)	C5—C6—N7—C8	-153 (8)
N1—C31—C32—O30	-54 (12)	C5—C6—N7—C71	78 (10)
N1—C31—C32—C33	-156 (9)	C5—C6—N7—LU1	-31 (9)
O30—C32—C33—N50	92 (7)	C9—C8—N7—C6	83 (12)
C31—C32—C33—N50	-176 (7)	C9—C8—N7—C71	-156 (11)
N4—C41—C42—O42	-172 (9)	C9—C8—N7—LU1	-41 (8)
N4—C41—C42—O41	-27 (18)	C72—C71—N7—C6	-86 (12)
N50—C60—C61—C62	-91 (6)	C72—C71—N7—C8	147 (9)
N50—C60—C61—C66	93 (6)	C72—C71—N7—LU1	28 (11)
C66—C61—C62—C63	12 (8)	C14—C13—N10—C11	154 (9)
C60—C61—C62—C63	-164 (5)	C14—C13—N10—C9	-52 (10)
C61—C62—C63—C64	-25 (15)	C14—C13—N10—LU1	42 (7)
C62—C63—C64—C65	15 (17)	C12—C11—N10—C13	-148 (9)
C63—C64—C65—C66	11 (10)	C12—C11—N10—C9	54 (7)
C64—C65—C66—C61	-16 (9)	C12—C11—N10—LU1	-37 (6)
C62—C61—C66—C65	4 (8)	C8—C9—N10—C13	33 (10)
C60—C61—C66—C65	180 (5)	C8—C9—N10—C11	-163 (5)
N7—C71—C72—O71	-0E1 (2)	C8—C9—N10—LU1	-63 (5)
N7—C71—C72—O72	148 (10)	C61—C60—N50—C50	-90 (13)
N7—C71—C72—LU1	-28 (12)	C61—C60—N50—C33	49 (8)
C3—C2—N1—C12	106 (6)	P51—C50—N50—C60	-144 (19)
C3—C2—N1—C31	-130 (7)	P51—C50—N50—C33	7E1 (2)
C3—C2—N1—LU1	-24 (8)	C32—C33—N50—C60	57 (10)
C11—C12—N1—C2	-174 (6)	C32—C33—N50—C50	-166 (13)
C11—C12—N1—C31	68 (7)	O12—C14—O11—LU1	161 (7)
C11—C12—N1—LU1	-40 (5)	C13—C14—O11—LU1	40 (11)
C32—C31—N1—C2	-163 (11)	C33—C32—O30—LU1	107 (6)

C32—C31—N1—C12	-53 (13)	C31—C32—O30—LU1	-2 (7)
C32—C31—N1—LU1	69 (11)	O42—C42—O41—LU1	158 (3)
C6—C5—N4—C41	-162 (7)	C41—C42—O41—LU1	0 (15)
C6—C5—N4—C3	-1E1 (2)	O72—C72—O71—LU1	176 (4)
C6—C5—N4—LU1	-66 (8)	C71—C72—O71—LU1	-35 (16)
C42—C41—N4—C5	129 (9)		

Table S6. Hydrogen-bond geometry (Å, º) for $\{(C(NH_2)_3)_2[Lu\mathbf{L_1}(H_2O)]\}\cdot 3H_2O$

D—H···*A*	*D*—H	H···*A*	*D*···*A*	*D*—H···*A*
C2—H2*B*···O41	0.97	2.66	3.0 (2)	101
C6—H6*B*···O72_$1^{i}	0.97	2.31	3.0 (2)	124
C8—H8*A*···O11	0.97	2.60	3.12 (19)	114
C8—H8*B*···O3W_$2^{ii}	0.97	2.56	3.4 (2)	148
C31—H31*A*···O42_$3^{iii}	0.97	2.69	3.27 (11)	119
C31—H31*B*···O41	0.97	2.61	3.02 (8)	106
C33—H33*A*···O51	0.97	2.66	3.31 (13)	125
C71—H71*B*···O11	0.97	2.14	2.71 (16)	116
N1*G*—H1*G*1···O1W_$4^{iv}	0.86	1.97	2.80 (15)	160
N1*G*—H1*G*2···O71_$4^{iv}	0.86	2.52	3.18 (12)	135
N2*G*—H2*G*1···O53	0.86	2.21	2.85 (12)	130
N2*G*—H2*G*2···O72_$4^{iv}	0.86	2.49	3.34 (18)	173
N3*G*—H3*G*1···O51	0.86	2.21	2.99 (11)	151
N3*G*—H3*G*2···O42	0.86	1.64	2.49 (13)	170
O30—H30···O52_$5^{v}	0.93	1.64	2.43 (14)	141
O1*W*—H11···O42_$4^{iv}	0.83 (8)	2.1 (4)	2.80 (10)	138 (54)
O2*W*—H22···O11	1.4 (5)	1.9 (2)	2.83 (14)	113 (30)
O2*W*—H22···O12	1.4 (5)	2.4 (4)	3.84 (19)	171 (24)
O3*W*—H32···O12_$5^{v}	1.2 (4)	2.0 (3)	2.93 (19)	128 (48)

Symmetry codes: (i) -*x*, -*y*, -*z*+1; (ii) *x*, *y*, *z*+1; (iii) -*x*+1, -*y*, -*z*; (iv) -*x*, -*y*, -*z*; (v) -*x*, -*y*+1, -*z*. Document origin: *publCIF*[S23]

VI. References

S1 L. Lattuada, R. Napolitano, V. Boi, M. Visigalli, S. Aime, G.B. Giovenzana, A. Fringuello Mingo, Contrast Agents, *Int. Pat. Appl. WO2017/09838*.

S2 H. C. Manning, M. Bai, B. M. Anderson, R. Lisiak, L. E. Samuelson, D. J. Bornhop, Expeditious synthesis of 'P'-protected macrocycles en route to lanthanide chelate metal complexes, *Tetrahedron Lett.* 2005, **46**, 4707-4710.

S3 J. M. Pagado, E. R. Goldberg, W. C. Fernelius, A thermodynamic study of homopiperazine, piperazine and *n*-(2-aminoethyl)-piperazine and their complexes with copper(II) ion, *Phys. Chem.*, 1961, **65**, 1062.

S4 K. Kumar, M. F. Tweedle, M. F.; Malley, J. Z. Gougoutas, Synthesis, Stability, and Crystal Structure Studies of Some Ca^{2+}, Cu^{2+}, and Zn^{2+} Complexes of Macrocyclic Polyamino Carboxylates *Inorg. Chem.* 1995, **34**, 6472.

S5 L. Leone, M. Boccalon, G. Ferrauto, I. Fábián, Zs. Baranyai, L. Tei, Acid-catalyzed proton exchange as a novel approach for relaxivity enhancement in Gd-HPDO3A-like complexes *Chem. Sci.*, 2020, **11**, 7829-7835

S6 É. Tóth, E. Brücher, I. Lázár, I. Tóth, Kinetics of Formation and Dissociation of Lanthanide(III)-DOTA Complexes, *Inorg. Chem.*, 1994, **33**, 4070.

S7 S. L. Wu, W. D. Horrocks, Kinetics of Complex Formation by Macrocyclic Polyaza Polycarboxylate Ligands: Detection and Characterization of an Intermediate in the Eu^{3+}-dota System by Laser-Excited Luminescence, *Inorg. Chem.*, 1995, **34**, 3724.

S8 J. Moreau, E. Guillon, J. C. Pierrard, J. Rimbault, M. Port, M. Aplincourt, Complexing Mechanism of the Lanthanide Cations Eu^{3+}, Gd^{3+}, and Tb^{3+} with 1,4,7,10‐Tetrakis(carboxymethyl)‐1,4,7,10‐tetraazacyclododecane (dota)—Characterization of Three Successive Complexing Phases: Study of the Thermodynamic and Structural Properties of the Complexes by Potentiometry, Luminescence Spectroscopy, and EXAFS *Chem. Eur. J.*, 2004, **10**, 5218.

S9 M. Perez-Malo, G. Szabo, E. Eppard, A. Vagner, E. Brucher, I. Toth, A. Maiocchi, E. H. Suh, Z. Kovacs, Z. Baranyai and F. Rosch, Improved Efficacy of Synthesizing *MIII-Labeled DOTA Complexes in Binary Mixtures of Water and Organic Solvents. A Combined Radio- and Physicochemical Study, *Inorg Chem*, 2018, **57**, 6107-6117

S10 A. Takács, R. Napolitano, M. Purgel, A. C. Bényei, L. Zékány, E. Brücher, I. Tóth, Z. Baranyai, S. Aime, Solution Structures, Stabilities, Kinetics, and Dynamics of DO3A and DO3A–Sulphonamide Complexes *Inorg. Chem.* 2014, **53**, 2858.

S11 A. E. Martell, S. M. Smith, *Critical stability constants* Vol 1-5. New York: Plenum Press; 1974-1982.

S12 R. Delgado and J.J.R.F. Da Silva, Metal complexes of cyclic tetra-azatetra-acetic acids *Talanta,*1982, **29**, 815.

S13 S. Aime, S. Baroni, D. Delli Castelli, E. Brücher, I. Fábián, S. Colombo Serra, A. Fringuello Mingo, R. Napolitano, L. Lattuada, F. Tedoldi, Z. Baranyai, Exploiting the Proton Exchange as an Additional Route to Enhance the Relaxivity of Paramagnetic MRI Contrast Agents, *Inorg. Chem.* 2018, **57**, 5567-5574

S14 K. Kumar, T. Jin, X. Wang, F. Desreux, M. F. Tweedle, Effect of Ligand Basicity on the Formation and Dissociation Equilibria and Kinetics of Gd^{3+} Complexes of Macrocyclic Polyamino Carboxylates, *Inorg. Chem.* 1994, **33**, 3823.

S15 L. Tei, Zs. Baranyai, L. Gaino, A. Forgács, A. Vágner, M. Botta, Thermodynamic stability, kinetic inertness and relaxometric properties of monoamide derivatives of lanthanide(III) DOTA complexes, *Dalton Trans.* 2015, 5467 – 5478.

S16 Z. Baranyai, Z. Pálinkás, F. Uggeri, A. Maiocchi, S. Aime and E. Brücher, Dissociation Kinetics of Open‐Chain and Macrocyclic Gadolinium(III)‐Aminopolycarboxylate Complexes Related to Magnetic Resonance Imaging: Catalytic Effect of Endogenous Ligands, *Chem. - Eur. J.*, 2012, **18**, 16426.

S17 A.C.T. North, D. C. Phillips, F. S. Mathews, A semi-empirical method of absorption correction, *Acta. Cryst.*1968, **A24**, 351.

S18 Enraf-Nonius, MACH3/PC Software. Enraf-Nonius, Delft, The Netherlands. 1995

S19 V. A. Streltsov, V. E. Zavodnik, PROFIT, *Sov. Phys. Crystallogr.* 1989, **34**, 824–828.

S20 A. Altomare, G. Cascarano, C. Giacovazzo, A. Guagliardi, M. C. Burla, G. Polidori, M. Camalli, SIR92 – a program for automatic solution of crystal structures by direct methods, *J. Appl. Cryst.*, 1994, **27**, 435.

S21 G. M. Sheldrick, A short history of SHELX, *Acta Cryst.* 2008, **A64**, 112–122.

S22 L. J. Farrugia, WinGX and ORTEP for Windows: an update, *J. Appl. Cryst.*, 2012, **45**, 849–854.

S23 S. P. Westrip, publCIF: software for editing, validating and formatting crystallographic information files, *J. Appl. Cryst.* 2010, **43**, 920–925.